Eur. Phys. J. Special Topics **160**, 319–330 (2008)

DOI: 10.1140/epjst/e2008-00735-6

THE EUROPEAN PHYSICAL JOURNAL SPECIAL TOPICS

Optimal continuous variable telecloning with bright entangled beams

S. Olivares[1,2,3,a] and M.G.A. Paris[3,4,b]

[1] CNISM, UdR Milano Università, 20133 Milano, Italy
[2] Dipartimento di Fisica e Matematica dell'Università dell'Insubria, 22100 Como, Italy
[3] Dipartimento di Fisica dell'Università di Milano, 20133 Milano, Italy
[4] Institute for Scientific Interchange, 10133 Torino, Italy

Abstract. We address continuous variable $1 \to 2$ telecloning based on three-mode entangled states of the radiation field. After reviewing existing protocols using phase-space formalism we suggest a novel scheme which allows telecloning with optimal fidelity also in the high energy regime. Being not limited by energy constraints our scheme is suitable to be implemented with feasible three-mode entanglement sources.

1 Introduction

Let us consider a situation where a sender wants to remotely provide an unknown quantum state of a continuous variable (CV) system to two distant receivers and he/she is not able to directly transfer neither the original state or the two copies (for the case in which direct transmission is a possible option see Refs. [1,2]). The most straightforward quantum mechanical strategy to achieve this goal requires two steps. One may first produce locally two copies of the original state by means of a cloning protocol. Then, the teleportation of each copy allows to attain the transfer of information. This strategy has the obvious advantage to use only bipartite entangled sources. Of course an analogous strategy in which the original state is firstly teleported and then cloned can be taken into account. However, in both cases and even in the absence of losses, the receivers are not left with two optimum clones of the original state, due to the non-unitary fidelity of the teleportation protocol in case of finite energy. This obstacle may be circumvented by pursuing a one-step strategy consisting of a nonlocal cloning. By this we mean that the cloning process is supported by a tripartite entangled state which is distributed among all the involved parties. This procedure is usually referred to as telecloning and represents a natural (nonlocal) generalization of the teleportation protocol to the many-recipient case [3–7].

CV teleportation is based on the twin-beam state obtained by parametric down-conversion, which provides the shared entanglement needed to support the protocol and to ensure optimal, even if non-unitary, fidelity for fixed input energy. Fidelity can be improved by using local operations and classical communication (LOCC) [8] or by performing conditional measurements on the twin beams [9,10]. Another optimized protocol for CV teleportation relies on a three-mode entangled state where one mode conditions the process by means of LOCC [11]. Twin beams are the coherent states of the group SU(1, 1) and thus, in order to implement a bipartite version of the teleportation protocol, one is naturally led to consider the coherent states of the group SU(2, 1). Indeed this has been recently analyzed by showing that telecloning with optimal fidelity is possible [12,13], at least when the overall energy of the entangled support is smaller

[a] e-mail: stefano.olivares@mi.infn.it
[b] e-mail: matteo.paris@fisica.unimi.it

than a given threshold. Other schemes involving cascading parametric interactions have been also investigated both theoretically and experimentally [14,15]. The telecloning protocol is a useful resource to share information among many parties by means of quantum communication channels [16], especially in the presence of noise [1].

In the following we will analyze in details $1 \to 2$ telecloning based on SU(2,1) three-mode entangled states of the radiation field. After reviewing existing protocols using phase-space formalism, we suggest a novel scheme which allows telecloning with optimal fidelity also in the high energy regime. Being not limited by energy constraints, this scheme is suitable to be implemented with current technology.

The three-mode entangled states of SU(2,1) are generated by the interaction Hamiltonian given by:

$$H_{\rm int} = \gamma_1 a_1^\dagger a_3^\dagger + \gamma_2 a_2^\dagger a_3 + \text{H.c.}\,, \tag{1}$$

where a_k and $a_k^\dagger$ are the annihilation and creation operators of the mode k, respectively, $[a_k, a_h^\dagger] = \delta_{kh}$. The Hamiltonian (1) describes two interlinked bilinear interactions among three modes of radiation in a $\chi^{(2)}$ nonlinear crystal. The effective couplings constants γ_1 and γ_2 of the two parametric processes are proportional to the nonlinear susceptibilities and the pump intensities [12,17]. Hamiltonian (1) admits the following constant of motion:

$$\hat{C} = \hat{N}_1 - (\hat{N}_2 + \hat{N}_3)\,, \quad \hat{N}_k = a_k^\dagger a_k\,, \tag{2}$$

and, if we take the vacuum as initial state, then we have $\langle \hat{C} \rangle = 0$ and the evolved three-mode state ϱ_{123} is a Gaussian state described by the characteristic function

$$\chi(\boldsymbol{\Lambda}) \equiv \chi[\varrho_{123}](\boldsymbol{\Lambda}) = \exp\left(-\tfrac{1}{2}\boldsymbol{\Lambda}^T \boldsymbol{\Sigma}\, \boldsymbol{\Lambda}\right)\,, \tag{3}$$

where $\boldsymbol{\Lambda} = (\boldsymbol{\Lambda}_1, \boldsymbol{\Lambda}_2, \boldsymbol{\Lambda}_3)^T \in \mathbb{R}^6$ is a column vector and the entries of the 6×6 covariance matrix $\boldsymbol{\Sigma}$ are given by $[\boldsymbol{\Sigma}]_{hk} = \frac{1}{2}\langle \{R_h, R_k\}\rangle - \langle R_k\rangle\langle R_h\rangle$, with $\boldsymbol{R} = (q_1, p_1, q_2, p_2, q_3, p_3)^T$, $q_k = \frac{1}{\sqrt{2}}(a_k + a_k^\dagger)$, $p_k = \frac{1}{i\sqrt{2}}(a_k - a_k^\dagger)$, and $\{R_h, R_k\} = R_h R_k + R_k R_h$. If we define the average number of photons $N_k = \text{Tr}[\varrho_{123}\hat{N}_k]$, then $\boldsymbol{\Sigma}$ can be written as follows ($k = 1,2,3$, $h = 2,3$):

$$\boldsymbol{\Sigma} = \begin{pmatrix} \boldsymbol{\mathcal{N}}_1 & \boldsymbol{\mathcal{A}}_{12} & \boldsymbol{\mathcal{A}}_{13} \\ \boldsymbol{\mathcal{A}}_{12}^T & \boldsymbol{\mathcal{N}}_2 & \boldsymbol{\mathcal{A}}_{23} \\ \boldsymbol{\mathcal{A}}_{13}^T & \boldsymbol{\mathcal{A}}_{23}^T & \boldsymbol{\mathcal{N}}_3 \end{pmatrix}, \qquad \begin{array}{l} \boldsymbol{\mathcal{N}}_k = \left(N_k + \frac{1}{2}\right)\mathbb{1}_2, \quad \boldsymbol{\mathcal{A}}_{1h} = \sqrt{(N_1+1)N_h}\,\mathbb{Q}\,(\phi_h), \\ \boldsymbol{\mathcal{A}}_{23} = -\sqrt{N_2 N_3}\,\mathbb{P}\,\mathbb{Q}\,(\phi_3 - \phi_2) \end{array} \tag{4}$$

where the entries are 2×2 real matrices, $\mathbb{1}_2$ is the 2×2 identity matrix,

$$\mathbb{Q}\,(\phi) = \begin{pmatrix} -\cos\phi & \sin\phi \\ \sin\phi & \cos\phi \end{pmatrix}, \tag{5}$$

$\mathbb{P} = \text{Diag}(1, -1)$, and ϕ_k are phases coming from the dynamics of the system itself [1,2,18, 19]. It is worth noting that when N_3 or N_2 vanishes the three-mode state (3) reduces to the two-mode twin-beam state of radiation.

The entanglement properties of the state (3) have been thoroughly investigated and, in particular, it has been shown that it is fully inseparable [2,17,19]. Moreover, if one considers the two-mode counterparts $\varrho_{hk} = \text{Tr}_l[\varrho_{123}]$, with $h \neq k \neq l$, one finds that whereas ϱ_{12} and ϱ_{13} are entangled, ϱ_{23} is separable [19]. As a consequence of the entanglement properties of the state (3), one can use it to implement $1 \to 2$ telecloning of an input state $\varrho_{\rm in}$ by jointly measuring it and mode 1 and acting on the left two modes by a suitable unitary transformation [12]. On the other hand, as we will see in the following, in this case the optimal fidelity (the similarity) between the input and the clones is achieved only if $N_1 = 2N_2 = 2N_3 = 1$, i.e., only if the state ϱ_{123} has a very low intensity: as N_1 increases, the fidelity decreases and falls below the classical limit $1/2$. In this paper we show a protocol that allows to implement optimal fidelity telecloning using high intensity three-mode states generated by (1). This is achieved by

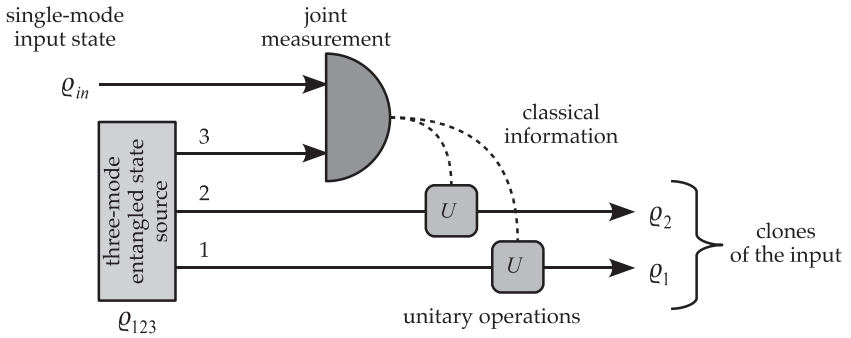

Fig. 1. General scheme of $1 \to 2$ telecloning: the single-mode input state $\varrho_{\rm in}$ undergoes a joint measurement with mode 3 of a three-mode entangled state. The result of the measurement is used to perform two unitary operations onto the remaining two modes, which become two clones of the input state.

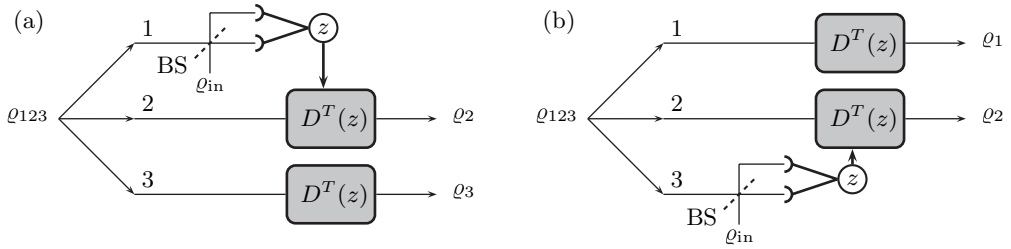

Fig. 2. Schemes of $1 \to 2$ telecloning: (a) the joint measurement is performed on mode 1; (b) the joint measurement is performed on mode 3. See the text for details.

tracing over one mode of the initial state and splitting one of the others by means of a beam splitter.

The paper is structured as follows. In section 2, by using the characteristic functions approach, we review the CV telecloning process addressing two possible measurement involving different modes of the shared state. Section 3 describes how to transform a state generated by the Hamiltonian (1) in a new three-mode state that allows optimal fidelity telecloning, also in regimes with $N_1 > 1$. The purity of the new state as well as its entanglement properties are also thoroughly investigated in this section. Section 4 closes the paper drawing some concluding remarks.

2 Continuous variable telecloning

In this section we review the telecloning process involving the state (3) as shared state. As depicted in Fig. 1, the input state $\varrho_{\rm in}$ and the mode 3 of the three-mode entangled state ϱ_{123} undergo a joint measurement, whose result is used as classical information to perform two unitary operations onto the remaining two modes, which are then converted into two clones of the input state. In the actual realization of the cloning protocol the joint measurement is achieved by means of double homodyne detection, whereas the unitary operations are displacement, thus the protocol can be recast as follows: one of the three modes of the shared state ϱ_{123} is mixed with $\varrho_{\rm in}$ at a balanced beam splitter (BS) and then a double homodyne detection is performed on the two emerging modes, getting, as outcome, a complex number z which is used to displace the remaining two modes of the shared state.

In Fig. 2 are sketched two possible schemes to implement the $1 \to 2$ telecloning protocol staring from the shared state ϱ_{123}: the only difference between the schemes is that in Fig. 2(a) the joint measurement is performed onto the mode 1, in Fig. 2(b) onto the mode 3 (the latter scheme is totally equivalent to perform the measurement onto mode 2).

2.1 Measurement involving mode 1

Let us focus our attention on the scheme of Fig. 2(a). If we assume that the input state is a Gaussian state with characteristic function

$$\chi_{\rm in}(\boldsymbol{\Lambda}_0) = \exp\left(-\tfrac{1}{2}\boldsymbol{\Lambda}_0^T\boldsymbol{\sigma}_{\rm in}\,\boldsymbol{\Lambda}_0 - i\boldsymbol{\Lambda}_0^T\overline{\boldsymbol{X}}\right), \tag{6}$$

then the positive operator-valued measure (POVM) of the double homodyne detection is given by [17]:

$$\mathit{\Pi}(z) = \pi^{-1}D(z)\varrho_{\rm in}^T D^\dagger(z)\,, \tag{7}$$

corresponding to the characteristic function (A.2) given in the Appendix A with:

$$\boldsymbol{\sigma}_{\rm M} = \mathbb{P}\,\boldsymbol{\sigma}_{\rm in}\mathbb{P}\,, \qquad \boldsymbol{X} = \mathbb{P}\,\overline{\boldsymbol{X}} + \boldsymbol{Z}\,, \tag{8}$$

where $\boldsymbol{Z} = \sqrt{2}(\mathrm{Re}[z], \mathrm{Im}[z])^T$. The characteristic function $\chi'(\tilde{\boldsymbol{\Lambda}})$ of the state $\varrho'_{23}(z)$ of modes 2 and 3 conditioned to the outcome z is given by Eq. (A.12) with $\tilde{\boldsymbol{\Lambda}} = (\boldsymbol{\Lambda}_2, \boldsymbol{\Lambda}_3)$ in Appendix A:

$$\boldsymbol{A} = \boldsymbol{\mathcal{N}}_1, \qquad \boldsymbol{B} = \begin{pmatrix} \boldsymbol{\mathcal{N}}_2 & \boldsymbol{\mathcal{A}}_{23} \\ \boldsymbol{\mathcal{A}}_{23}^T & \boldsymbol{\mathcal{N}}_3 \end{pmatrix}, \qquad \boldsymbol{C} = \begin{pmatrix} \boldsymbol{\mathcal{A}}_{12} & \boldsymbol{\mathcal{A}}_{13} \end{pmatrix}, \tag{9}$$

and the probability $p(\boldsymbol{Z})$ of the outcome z follows from Eq. (A.6). After the measurement we have to displace the conditioned state, i.e.,

$$\varrho'_{23} \to \tilde{\varrho}'_{23}(z) \equiv U_z\varrho'_{23}(z)U_z^\dagger, \tag{10}$$

with $U_z = D^T(z) \otimes D^T(z)$; the corresponding characteristic function $\tilde{\chi}'(\tilde{\boldsymbol{\Lambda}})$ reads

$$\tilde{\chi}'(\tilde{\boldsymbol{\Lambda}}) = \chi'(\tilde{\boldsymbol{\Lambda}})\exp\left(i\tilde{\boldsymbol{\Lambda}}^T\mathbb{J}^T\mathbb{P}\,\boldsymbol{Z}\right), \tag{11}$$

with $\mathbb{J} = (\mathbb{1}_2, \mathbb{1}_2)$. The two mode output state is obtained averaging Eq. (11) over z, i.e.,

$$\chi'_{\rm out}(\tilde{\boldsymbol{\Lambda}}) = \int_{\mathbb{R}^2}\frac{d^2\boldsymbol{Z}}{2}p(\boldsymbol{Z})\,\tilde{\chi}'(\tilde{\boldsymbol{\Lambda}}) \tag{12}$$

$$= \exp\left[-\tfrac{1}{2}\tilde{\boldsymbol{\Lambda}}^T\left(\mathbb{J}^T\boldsymbol{\sigma}_{\rm in}\mathbb{J} + \boldsymbol{B} + \mathbb{J}^T\mathbb{P}\,\boldsymbol{A}\mathbb{P}\,\mathbb{J} - \mathbb{J}^T\mathbb{P}\,\boldsymbol{C} - \boldsymbol{C}^T\mathbb{P}\,\mathbb{J}\right)\tilde{\boldsymbol{\Lambda}} - i\tilde{\boldsymbol{\Lambda}}^T\mathbb{J}^T\overline{\boldsymbol{X}}\right], \tag{13}$$

where we used Eqs. (8). The state of mode $h = 2, 3$ is then described by the characteristic function

$$\chi_h(\boldsymbol{\Lambda}_h) = \int_{\mathbb{R}^2}\frac{d^2\boldsymbol{\Lambda}_h}{2\pi}\,\chi'_{\rm out}(\boldsymbol{\Lambda}_1, \boldsymbol{\Lambda}_2)\,(2\pi)\delta^{(2)}(\boldsymbol{\Lambda}_k), \tag{14}$$

with $k = 2, 3$, $k \neq h$, i.e., the clones are Gaussian states with mean value vector $\overline{\boldsymbol{X}}$ and covariance matrices given by:

$$\boldsymbol{\sigma}_h = \boldsymbol{\sigma}_{\rm in} + \mathbb{P}\boldsymbol{\mathcal{N}}_1\mathbb{P} + \boldsymbol{\mathcal{N}}_h - \mathbb{P}\,\boldsymbol{\mathcal{A}}_{1h} - \boldsymbol{\mathcal{A}}_{1h}^T\mathbb{P}\,. \tag{15}$$

As usual, the clone fidelity, i.e., the similarity between the input state and the clone corresponding to mode h, is defined as:

$$F_{1h} = \int_{\mathbb{R}^2}\frac{d^2\boldsymbol{\Lambda}_h}{2\pi}\chi_h(\boldsymbol{\Lambda}_h)\,\chi_{\rm in}(-\boldsymbol{\Lambda}_h) = \{\mathrm{Det}[\boldsymbol{\sigma}_h + \boldsymbol{\sigma}_{\rm in}]\}^{-1/2} \tag{16}$$

$$= \left[2 + N_1 + N_h + 2\sqrt{N_h(1+N_1)}\cos\phi_h\right]^{-1}, \tag{17}$$

which reaches the maximum for $\phi_h = \pi$.

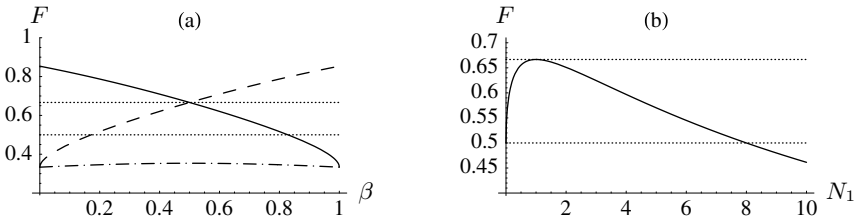

Fig. 3. (a) Plots of the cloning fidelities F_{12} (solid line), $F_{13} = F_{31}$ (dashed line) and F_{32} (dot-dashed line) as functions of the parameter β with $N_1 = 1$ (see the text for details). (b) Plot of the cloning fidelity in the case of symmetric cloning, i.e., $\beta = 1/2$, as a function N_1. The dotted lines refer to $F = 1/2$ and $F = 2/3$. We set $\phi_2 = \phi_3 = \pi$.

2.2 Measurement involving mode 3

Let us now turn our attention on Fig. 2(b). Now we have that the characteristic function $\chi''(\tilde{\boldsymbol{\Lambda}})$ of the state $\varrho''_{12}(z)$ of modes 1 and 2 conditioned to the outcome z is given by Eq. (A.23) with $\tilde{\boldsymbol{\Lambda}} = (\boldsymbol{\Lambda}_1, \boldsymbol{\Lambda}_2)$ in Appendix A:

$$\boldsymbol{B} = \boldsymbol{\mathcal{N}}_3, \qquad \boldsymbol{A} = \begin{pmatrix} \boldsymbol{\mathcal{N}}_1 & \boldsymbol{\mathcal{A}}_{12} \\ \boldsymbol{\mathcal{A}}_{12}^T & \boldsymbol{\mathcal{N}}_2 \end{pmatrix}, \qquad \boldsymbol{C}^T = \begin{pmatrix} \boldsymbol{\mathcal{A}}_{13}^T & \boldsymbol{\mathcal{B}}_{23}^T \end{pmatrix}, \tag{18}$$

and the probability $p(\boldsymbol{Z})$ follows from Eq. (A.17). *Mutatis mutandis*, after the displacements and the averaging over z one gets

$$\chi''_{\rm out}(\tilde{\boldsymbol{\Lambda}}) = \exp\left[-\tfrac{1}{2}\tilde{\boldsymbol{\Lambda}}^T\left(\mathbb{J}^T\boldsymbol{\sigma}_{\rm in}\mathbb{J} + \boldsymbol{A} + \mathbb{J}^T\mathbb{P}\,\boldsymbol{B}\mathbb{P}\,\mathbb{J} - \mathbb{J}^T\mathbb{P}\,\boldsymbol{C}^T - \boldsymbol{C}\mathbb{P}\,\mathbb{J}\right)\tilde{\boldsymbol{\Lambda}} - i\tilde{\boldsymbol{\Lambda}}^T\mathbb{J}^T\overline{\boldsymbol{X}}\right], \tag{19}$$

and the clones are still Gaussian states with mean value vector $\overline{\boldsymbol{X}}$ and covariance matrices given by

$$\boldsymbol{\sigma}_k = \boldsymbol{\sigma}_{\rm in} + \mathbb{P}\,\boldsymbol{\mathcal{N}}_3\mathbb{P} + \boldsymbol{\mathcal{N}}_k - \mathbb{P}\,\boldsymbol{\mathcal{A}}_{k3}^T - \boldsymbol{\mathcal{A}}_{k3}\mathbb{P}, \tag{20}$$

with $k = 1, 2$. Finally, the cloning fidelities F_{3k}, $k = 1, 2$, read as follows:

$$F_{31} = \left[2 + N_1 + N_3 + 2\sqrt{N_3(1+N_1)}\cos\phi_3\right]^{-1}, \tag{21}$$

$$F_{32} = \left[(2 + N_2 + N_3)^2 - 4N_2N_3\right]^{-1/2}. \tag{22}$$

As in the previous case, F_{31} reaches the maximum for $\phi_3 = \pi$, whereas $F_{32} \leq 1/2$: this is due to the fact that the two-mode state $\varrho_{23} = {\rm Tr}_1[\varrho_{123}]$ is a separable state [19]. Note that $F_{13} = F_{31}$.

2.3 Discussion

In Fig. 3(a) we plot F_{12}, $F_{13} = F_{31}$ and F_{32} as functions of the parameter $\beta \in [0, 1]$ such that

$$N_2 = (1-\beta)N_1, \qquad N_3 = \beta N_1, \tag{23}$$

with $N_1 = 1$: in this case, when $\beta = 1/2$ we achieve the optimal symmetric cloning fidelity, i.e., $F_{12} = F_{13} = 2/3$. As mentioned above, F_{32} is always less than $1/2$, whereas, varying β, one can increase the fidelity of one clone with respect to the other one. In the case of symmetric cloning, i.e., $\beta = 1/2$, we have

$$F_{12} = F_{13} \equiv F(N_1) = \left[2 + \frac{3}{2}N_1 - \sqrt{2N_1(1+N_1)}\right]^{-1}, \tag{24}$$

which is plotted in Fig. 3(b): we can see that the maximum is achieved for $N_1 = 1$, whereas the fidelity falls below the classical value $F = 1/2$ for $N_1 \geq 8$.

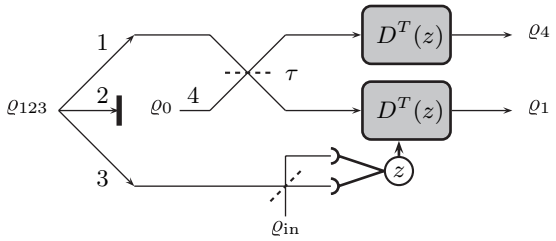

Fig. 4. Scheme to implement $1 \to 2$ optimal telecloning with high intensity beams.

3 Telecloning with bright beams

As pointed out in the previous section, when the three-mode entangled state shared between the three parties is the Gaussian state (3) with covariance matrix (4), the optimal symmetric cloning fidelity, i.e., $F = 2/3$, is achieved only if $N_1 = 1$ (and $N_2 = N_3 = 1/2$). Moreover, if $N_1 \geq 8$ then $F \leq 1/2$: this states that high intensity beams described by Eq. (3) cannot be used to implement telecloning. Nonetheless, in this section we show how it is possible to obtain optimal telecloning with three-mode states with $N_1 > 1$ by eliminating one of mode 2 or 3 and by dividing mode 1 into two beams by means of a BS. The protocol is depicted in Fig. 4. The mode 2 of the shared state ϱ_{123} is absorbed, whereas mode 1 is mixed with the vacuum state ϱ_0 of mode 4 in a BS with transmissivity τ: this generates a new three-mode state and, then, the telecloning protocol proceeds as in Fig. 2(b) and described in section 2.

The characteristic function of the state $\varrho_{13} = \mathrm{Tr}_2[\varrho_{123}]$ is still a Gaussian function which reads as follows

$$\chi[\varrho_{13}](\boldsymbol{\Lambda}_1, \boldsymbol{\Lambda}_3) = \int_{\mathbb{R}^2} \frac{d^2\boldsymbol{\Lambda}_2}{2\pi}\, \chi(\boldsymbol{\Lambda})\, (2\pi)\delta^{(2)}(-\boldsymbol{\Lambda}_2)\,, \tag{25}$$

where $\boldsymbol{\Lambda} = (\boldsymbol{\Lambda}_1, \boldsymbol{\Lambda}_2, \boldsymbol{\Lambda}_3)$ and $\chi(\boldsymbol{\Lambda})$ is given in Eq. (3). Now, the characteristic function of the states $\varrho_{134} = \varrho_{13} \otimes \varrho_0$, ϱ_0 being the vacuum state of mode 4, can be written as $\bar{\chi}(\bar{\boldsymbol{\Lambda}}) = \exp\left(-\frac{1}{2}\bar{\boldsymbol{\Lambda}}^T \bar{\boldsymbol{\Sigma}}\, \bar{\boldsymbol{\Lambda}}\right)$ where $\bar{\boldsymbol{\Lambda}} = (\boldsymbol{\Lambda}_1, \boldsymbol{\Lambda}_4, \boldsymbol{\Lambda}_3)$, the subscripts referring to the corresponding mode, and

$$\bar{\boldsymbol{\Sigma}} = \begin{pmatrix} \boldsymbol{\mathcal{N}}_1 & \mathbf{0} & \boldsymbol{\mathcal{A}}_{13} \\ \mathbf{0} & \boldsymbol{\sigma}_0 & \mathbf{0} \\ \boldsymbol{\mathcal{A}}_{13}^T & \mathbf{0} & \boldsymbol{\mathcal{N}}_3 \end{pmatrix}, \tag{26}$$

$\boldsymbol{\sigma}_0 = \frac{1}{2}\mathbb{1}_2$ being the covariance matrix of the vacuum state. In the covariance matrix (26) we rearranged the order of the modes in such a way that, formally, mode 4 replaces mode 2 in Eq. (3): this choice allows us to use the results obtained in section 2. The next step of the protocol is to mix mode 1 and 4 at a BS with transmissivity τ (see Fig. 4). Since we are dealing with a Gaussian state, this operation onto mode 1 and 4 reduces to a transformation of the covariance matrix (26) as follows (the transformed state is still Gaussian):

$$\bar{\boldsymbol{\Sigma}} \to \boldsymbol{\Theta} = \boldsymbol{S}_\tau^T\, \bar{\boldsymbol{\Sigma}}\, \boldsymbol{S}_\tau\,, \tag{27}$$

where

$$\boldsymbol{S}_\tau = \left(\begin{array}{c|c} \boldsymbol{S}_{\rm BS}(\tau) & \mathbf{0} \\ \hline \mathbf{0} & \mathbb{1}_2 \end{array}\right), \qquad \boldsymbol{S}_{\rm BS}(\tau) = \left(\begin{array}{c|c} \sqrt{\tau}\mathbb{1}_2 & \sqrt{1-\tau}\mathbb{1}_2 \\ \hline -\sqrt{1-\tau}\mathbb{1}_2 & \sqrt{\tau}\mathbb{1}_2 \end{array}\right). \tag{28}$$

Analogously to Eq. (4), we write the explicit form of the covariance matrix $\boldsymbol{\Theta}$ as

$$\boldsymbol{\Theta} = \begin{pmatrix} \boldsymbol{\mathcal{M}}_1 & \boldsymbol{\mathcal{B}}_{14} & \boldsymbol{\mathcal{B}}_{13} \\ \boldsymbol{\mathcal{B}}_{14}^T & \boldsymbol{\mathcal{M}}_4 & \boldsymbol{\mathcal{B}}_{43} \\ \boldsymbol{\mathcal{B}}_{13}^T & \boldsymbol{\mathcal{B}}_{43}^T & \boldsymbol{\mathcal{M}}_3 \end{pmatrix}, \tag{29}$$

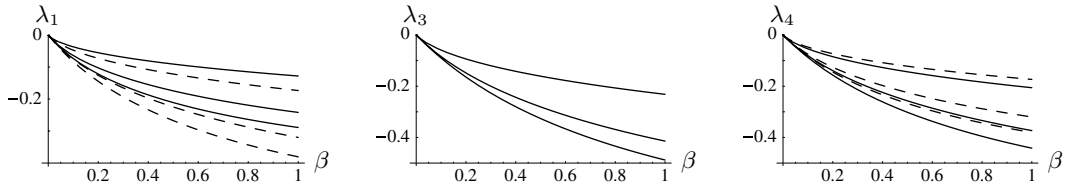

Fig. 5. Plots of the minimum eigenvalue λ_k of $\boldsymbol{\Theta} - \frac{i}{2}\boldsymbol{\Omega}(k)$, $k = 1, 3, 4$, as a function of β and different values of N_1 (from top to bottom in each plot: $N_1 = 0.1, 1$ and 10) and τ: the solid lines refer to $\tau = 0.25$, the dashed lines to $\tau = 0.5$ (λ_3 does not depend on τ).

where the entries are 2×2 real matrices given by:

$$\boldsymbol{\mathcal{M}}_1 = \left(N_1\tau + \tfrac{1}{2}\right)\mathbb{1}_2, \quad \boldsymbol{\mathcal{M}}_4 = \left[N_1(1-\tau) + \tfrac{1}{2}\right]\mathbb{1}_2, \quad \boldsymbol{\mathcal{M}}_3 = \boldsymbol{\mathcal{N}}_3 = \left(\beta N_1 + \tfrac{1}{2}\right)\mathbb{1}_2, \tag{30a}$$

$$\boldsymbol{\mathcal{B}}_{14} = N_1\sqrt{1-\tau^2}\,\mathbb{Q}\,(\phi_3), \quad \boldsymbol{\mathcal{B}}_{13} = \sqrt{\tau\beta N_1(N_1+1)}\,\mathbb{Q}\,(\phi_3), \tag{30b}$$

$$\boldsymbol{\mathcal{B}}_{43} = \sqrt{(1-\tau)\beta N_1(N_1+1)}\,\mathbb{Q}\,(\phi_3), \tag{30c}$$

and we used Eqs. (23).

3.1 State characterization

The three-mode Gaussian state ϱ_{134} is fully characterized by its covariance matrix $\boldsymbol{\Theta}$. The first quantity we are interested in is the purity $\mu = (64\sqrt{\mathrm{Det}[\boldsymbol{\Theta}]})^{-1}$, that is:

$$\mu(E_{\rm tot}, \beta) = \frac{1+\beta}{1+\beta+2E_{\rm tot}(1-\beta)}, \tag{31}$$

where we defined the total energy $E_{\rm tot} = N_1(1+\beta)$. As one may expect the purity becomes smaller as $E_{\rm tot}$ increases and $\beta < 1$ (if $\beta = 1$ then $\mu = 1$, since mode 2 was in the vacuum state).

Let us now focus our attention on the separability. Since we are dealing with a Gaussian state, its separability can be investigated by means of the positivity of the partial transpose (PPT) [20]. For a three-mode state the only partially separable forms are those with a bipartite splitting of 1×2 modes, thus the PPT with respect to mode $k = 1, 3, 4$, can be written as

$$\boldsymbol{\Theta} + \frac{i}{2}\boldsymbol{\Omega}(k) \geq 0, \quad \text{with} \quad \boldsymbol{\Omega}(k) = \begin{pmatrix} f_{1,k}\,\boldsymbol{\omega} & \mathbf{0} & \mathbf{0} \\ \mathbf{0} & f_{4,k}\,\boldsymbol{\omega} & \mathbf{0} \\ \mathbf{0} & \mathbf{0} & f_{3,k}\,\boldsymbol{\omega} \end{pmatrix}, \quad \boldsymbol{\omega} = \begin{pmatrix} 0 & 1 \\ -1 & 0 \end{pmatrix}. \tag{32}$$

where $f_{h,k} = 1 - 2\delta_{h,k}$. In Fig. 5 we plot the minimum eigenvalue λ_k of $\boldsymbol{\Theta} + \frac{i}{2}\boldsymbol{\Omega}(k)$, $k = 1, 3, 4$, as a function of β and different values of N_1 and τ: since $\lambda_k < 0\ \forall k$, we conclude that ϱ_{134} is fully inseparable. The state becomes separable only if $\beta = 0$, i.e., mode 3 is initially in the vacuum state.

In the following, we investigate the separability of the two-mode states obtained from ϱ_{134} tracing over one of the three modes. Since the characteristic function of the state ϱ_{134}, i.e., $\chi[\varrho_{134}](\bar{\boldsymbol{\Lambda}}) = \exp(-\frac{1}{2}\bar{\boldsymbol{\Lambda}}^T\bar{\boldsymbol{\Theta}}\,\bar{\boldsymbol{\Lambda}})$, is Gaussian, when we trace over one mode, the resulting two-mode state is still Gaussian, and its separability can be investigated by means of the PPT criterion that, now, reads as follows [20]:

$$\boldsymbol{\Theta}_{hk} + \frac{i}{2}\tilde{\boldsymbol{\Omega}} \geq 0, \qquad \tilde{\boldsymbol{\Omega}} = \begin{pmatrix} \boldsymbol{\omega} & \mathbf{0} \\ \mathbf{0} & -\boldsymbol{\omega} \end{pmatrix}, \tag{33}$$

where $\boldsymbol{\Theta}_{hk}$ is the 4×4 covariance matrix of the two-mode state obtained tracing over mode $l \neq h, k$. When the inequality in (33) is verified, then mode h and k are separable. In Fig. 6 we plot the minimum eigenvalue γ_{hk} of the left hand side of the inequality in (33) as a function of β and different values of N_1 and τ: as one may expect, modes 1 and 4 are always separable, whereas the subsystems 1–3 and 3–4 are entangled.

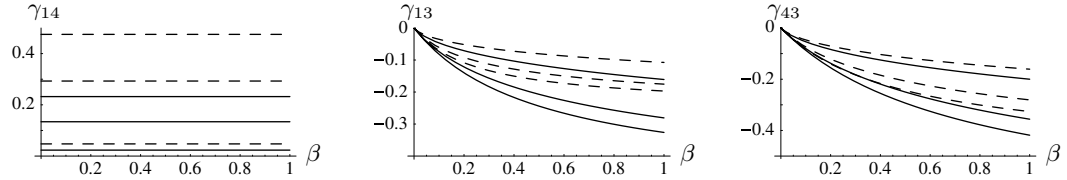

Fig. 6. Plots of the minimum eigenvalue γ_{hk} of $\boldsymbol{\Theta}_{hk} + \frac{i}{2}\tilde{\boldsymbol{\Omega}}$, $h, k = 1, 3, 4$, $h \neq k$, as a function of β and different values of N_1 (from bottom to top for γ_{14} and from top to bottom for γ_{13} and γ_{14}: $N_1 = 0.1, 1$ and 10) and τ: the solid lines refer to $\tau = 0.25$, the dashed lines to $\tau = 0.5$.

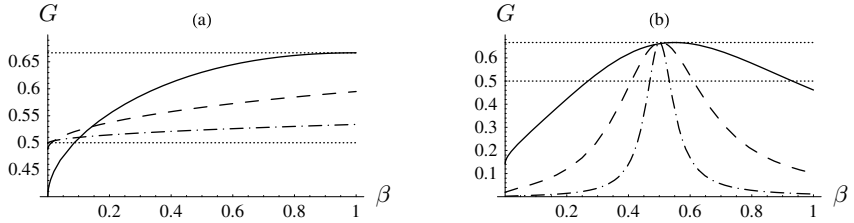

Fig. 7. Plot of the cloning fidelity $G = G_{31} = G_{34}$ in the case of symmetric cloning, i.e., $\tau = 0.5$, in the two regimes (a) $0 \leq N_1 \leq 1$ and (b) $N_1 > 1$ as a function of β and different values of N_1: (a) $N_1 = 0.01$ (dot-dashed line), 0.1 (dashed line) and 1 (solid line), (b) and $N_1 = 1000$ (dot-dashed line), 100 (dashed line) and 10 (solid line). The dotted lines refer to $G = 1/2$ and $G = 2/3$. We set $\phi_3 = \pi$.

3.2 Telecloning

Since mode 1 and 4 are not entangled, here we address the telecloning process from mode 3 to mode 1 and 4. The calculation is similar to that of section 2.2, but, now, the two Gaussian clones, i.e., ϱ_1 and ϱ_4 (see Fig. 4), have the following covariance matrix $\boldsymbol{\theta}_k$, $k = 1, 4$:

$$\boldsymbol{\theta}_k = \boldsymbol{\sigma}_{\rm in} + \mathbb{P}\,\boldsymbol{\mathcal{M}}_3\mathbb{P} + \boldsymbol{\mathcal{M}}_k - \mathbb{P}\,\boldsymbol{\mathcal{B}}_{k3}^T - \boldsymbol{\mathcal{B}}_{k3}\mathbb{P}\,. \tag{34}$$

Now, the cloning fidelities $G_{3k} = \{\mathrm{Det}[\sqrt{\boldsymbol{\sigma}_{\rm in} + \boldsymbol{\theta}_k}]\}^{-1}$, $k = 1, 4$, are given by:

$$G_{31} = \left[2 + N_1(\tau + \beta) + 2\sqrt{\beta\tau N_1(1 + N_1)}\cos\phi_3\right]^{-1}, \tag{35}$$

$$G_{34} = \left[2 + N_1(1 - \tau + \beta) + 2\sqrt{\beta(1 - \tau)N_1(1 + N_1)}\cos\phi_3\right]^{-1}, \tag{36}$$

where we used $N_1 = \beta N_1$. Note that the fidelities are maxima for $\phi_3 = \pi$, as in the previous cases (see section 2).

In the following we focus the attention on the symmetric cloning setup, i.e., $\tau = 0.5$: in this case mode 1 and 4 of the state ϱ_{134} have the same energy and $G_{31} = G_{34} = G$. As one can see in Fig. 7, we can distinguish two regimes with respect to the value of N_1: (a) $0 \leq N_1 \leq 1$ and (b) $N_1 > 1$. In regime (a) the optimal symmetric cloning $G = 2/3$ is achieved only for $\beta = 1$ and $N_1 = 1$. In regime (b) G *always* reaches the maximum value 2/3 for $\beta = (1 + N_1)/(2N_1)$. In both the regimes, $G > 1/2$ if:

$$\frac{2 + N_1 - 2\sqrt{1 + N_1}}{2N_1} < \beta < \mathrm{Min}\left[1, \frac{2 + N_1 + 2\sqrt{1 + N_1}}{2N_1}\right]. \tag{37}$$

Note that as N_1 increases the interval (37) becomes smaller and smaller. Figure 8 shows G as a function of N_1 for different values of β. We can see that for $0.5 \leq \beta \leq 1$ the fidelity G always reaches the optimal value 2/3 at $N_1 = (2\beta - 1)^{-1}$. As one may expect, for $0 \leq \beta < 0.5$ the fidelity never reaches 2/3 and the maximum is obtained for $N_1 = 2\beta/(1 - 2\beta)$.

In Fig. 9 the symmetric cloning fidelity G is plotted as a function of the total energy and the purity of the state ϱ_{134}.

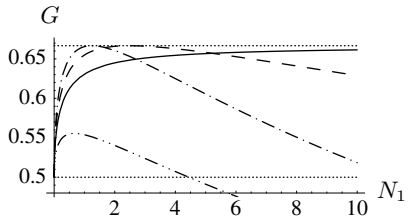

Fig. 8. Plot of the cloning fidelity $G = G_{31} = G_{34}$ in the case of symmetric cloning, i.e., $\tau = 0.5$, as a function of N_1 and different values of β: $\beta = 0.9$ (dot-dashed line), 0.7 (dashed line), 0.5 (solid line), and 0.2 (dot-dot-dashed line). The dotted lines refer to $G = 1/2$ and $G = 2/3$. We set $\phi_3 = \pi$.

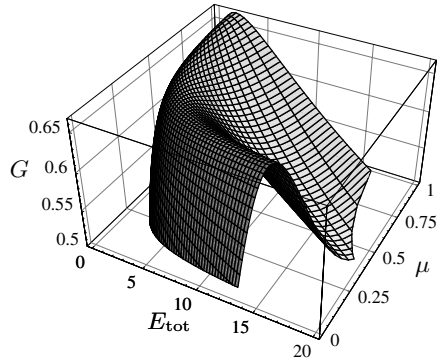

Fig. 9. Plot of the cloning fidelity $G = G_{31} = G_{34}$ in the case of symmetric cloning, i.e., $\tau = 0.5$, as a function of the total energy $E_{\rm tot}$ and the purity μ of the state ϱ_{134}. We set $\phi_3 = \pi$.

4 Conclusions

We have addressed continuous variable $1 \to 2$ telecloning based on three-mode entangled states of the radiation field. After reviewing existing protocols using phase-space formalism we have suggested a novel scheme which allows telecloning with optimal fidelity also in the high energy regime. Our scheme is based on a novel entangled state synthesized by linear optical elements and absorption starting from the SU(2,1) three-mode state obtained from two interlinked bilinear interactions in a $\chi^{(2)}$ nonlinear crystal. We have analyzed purity and entanglement of the novel state and evaluated the telecloning fidelity in different regimes, thus showing that optimal telecloning is possibile also when the average photon number of the shared state is large. Finally, we notice that being not limited by energy constraints our scheme is suitable to be implemented with current technology, i.e., by using feasible schemes to generate three-mode entanglement, based on nonlinear crystals, already demonstrated experimentally [12,13].

This work was supported by MIUR through the project PRIN-2005024254-002 and by the CNR-CNISM convention.

Appendix

A Conditional measurement onto a n-mode Gaussian state

Let us consider the following Gaussian characteristic function with zero mean value associated with a n-mode state:

$$\chi(\boldsymbol{\Lambda}) = \exp\left(-\tfrac{1}{2}\boldsymbol{\Lambda}^T \boldsymbol{\Sigma}\, \boldsymbol{\Lambda}\right) , \tag{A.1}$$

where $\boldsymbol{\Lambda} = (\boldsymbol{\Lambda}_1, \boldsymbol{\Lambda}_2, \ldots, \boldsymbol{\Lambda}_n) \in \mathbb{R}^{2n}$ is a column vector and $\boldsymbol{\Sigma}$ is the $2n \times 2n$ covariance matrix $[\boldsymbol{\Sigma}]_{h,k} = \frac{1}{2}\langle\{R_h, R_k\}\rangle - \langle R_h\rangle\langle R_k\rangle$ with $\boldsymbol{R} = (q_1, p_1, \ldots, q_n, p_n)^T$, $q_k = \frac{1}{\sqrt{2}}(a_k + a_k^\dagger)$ and $p_k = \frac{1}{i\sqrt{2}}(a_k - a_k^\dagger)$, a_k being the field operator of mode k, and $\{R_h, R_k\} = R_h R_k + R_k R_h$.

Measurement on mode 1 — In the following we are interested in performing on mode 1 a measurement described by the characteristic function

$$\chi_{\mathrm{M}}(\boldsymbol{\Lambda}_1) = \pi^{-1} \exp\left(-\tfrac{1}{2}\boldsymbol{\Lambda}_1^T \boldsymbol{\sigma}_{\mathrm{M}}\, \boldsymbol{\Lambda}_1 - i\boldsymbol{\Lambda}_1^T \boldsymbol{X}\right), \tag{A.2}$$

where $\boldsymbol{\sigma}_{\mathrm{M}}$ is the covariance matrix of the measurement and $\boldsymbol{X}$ the mean values vector. For the sake of simplicity, we write the vector $\boldsymbol{\Lambda}$ and the covariance matrix $\boldsymbol{\Sigma}$ as follows:

$$\boldsymbol{\Lambda} = (\boldsymbol{\Lambda}_1, \boldsymbol{\Lambda}_2, \ldots, \boldsymbol{\Lambda}_n) = (\boldsymbol{\Lambda}_1, \tilde{\boldsymbol{\Lambda}}), \quad \boldsymbol{\Sigma} = \left(\begin{array}{c|c} \boldsymbol{A} & \boldsymbol{C} \\ \hline \boldsymbol{C}^T & \boldsymbol{B} \end{array}\right), \tag{A.3}$$

where $\boldsymbol{A} \in \mathbb{R}^2 \times \mathbb{R}^2$ and $\boldsymbol{B} \in \mathbb{R}^2 \times \mathbb{R}^{2(n-1)}$ are symmetric, and $\boldsymbol{C} \in \mathbb{R}^2 \times \mathbb{R}^{2(n-1)}$. The characteristic function of the system after the measurement is given by

$$\chi'(\tilde{\boldsymbol{\Lambda}}) = \frac{1}{p(\boldsymbol{X})} \int_{\mathbb{R}^2} \frac{d^2\boldsymbol{\Lambda}_1}{2\pi} \chi(\boldsymbol{\Lambda}_1, \tilde{\boldsymbol{\Lambda}})\, \chi_{\mathrm{M}}(-\boldsymbol{\Lambda}_1), \tag{A.4}$$

$p(\boldsymbol{X})$ being the probability of the outcome $\boldsymbol{X}$:

$$p(\boldsymbol{X}) = \frac{1}{(2\pi)^n} \int_{\mathbb{R}^{2n}} d^2\boldsymbol{\Lambda}_1\, d^{2(n-1)}\tilde{\boldsymbol{\Lambda}}\, \chi(\boldsymbol{\Lambda}_1, \tilde{\boldsymbol{\Lambda}}) \times \chi_{\mathrm{M}}(-\boldsymbol{\Lambda}_1)\, (2\pi)^{2(n-1)} \delta(-\tilde{\boldsymbol{\Lambda}}) \tag{A.5}$$

$$= \int_{\mathbb{R}^2} \frac{d^2\boldsymbol{\Lambda}_1}{2\pi^2} \exp\left[-\tfrac{1}{2}\boldsymbol{\Lambda}_1^T(\boldsymbol{A} + \boldsymbol{\sigma}_{\mathrm{M}})\, \boldsymbol{\Lambda}_1 + i\boldsymbol{\Lambda}_1^T \boldsymbol{X}\right] = \frac{\exp\left[-\frac{1}{2}\boldsymbol{X}^T(\boldsymbol{A} + \boldsymbol{\sigma}_{\mathrm{M}})^{-1}\, \boldsymbol{X}\right]}{\pi\sqrt{\mathrm{Det}[\boldsymbol{A} + \boldsymbol{\sigma}_{\mathrm{M}}]}}, \tag{A.6}$$

where $\delta(-\tilde{\boldsymbol{\Lambda}}) = \prod_{k=2}^n \delta^{(2)}(-\boldsymbol{\Lambda}_k)$ is the product of Kronecker deltas in $\mathbb{R}^2$. Note that

$$\chi(\boldsymbol{\Lambda}_1, \tilde{\boldsymbol{\Lambda}})\, \chi_{\mathrm{M}}(-\boldsymbol{\Lambda}_1) = \pi^{-1} \exp\left[-\tfrac{1}{2}(\boldsymbol{\Lambda}_1, \tilde{\boldsymbol{\Lambda}})^T \boldsymbol{\sigma}\, (\boldsymbol{\Lambda}_1, \tilde{\boldsymbol{\Lambda}}) + i\boldsymbol{\Lambda}_1^T \boldsymbol{X}\right], \tag{A.7}$$

where

$$\boldsymbol{\sigma} = \left(\begin{array}{c|c} \boldsymbol{A} + \boldsymbol{\sigma}_{\mathrm{M}} & \boldsymbol{C} \\ \hline \boldsymbol{C}^T & \boldsymbol{B} \end{array}\right). \tag{A.8}$$

In order to perform the integral (A.4) we observe that $\boldsymbol{\sigma}$ can be rewritten as follows:

$$\boldsymbol{\sigma} = \boldsymbol{M}^T \left(\begin{array}{c|c} \boldsymbol{A} + \boldsymbol{\sigma}_{\mathrm{M}} & \boldsymbol{0} \\ \hline \boldsymbol{0} & \boldsymbol{B} - \boldsymbol{C}^T(\boldsymbol{A} + \boldsymbol{\sigma}_{\mathrm{M}})^{-1}\boldsymbol{C} \end{array}\right) \boldsymbol{M}, \quad \boldsymbol{M} = \left(\begin{array}{c|c} \mathbb{1}_2 & (\boldsymbol{A} + \boldsymbol{\sigma}_{\mathrm{M}})^{-1}\boldsymbol{C} \\ \hline \boldsymbol{0} & \mathbb{1}_{2(n-1)} \end{array}\right), \tag{A.9}$$

where $\mathbb{1}_k$ is the $k \times k$ identity matrix and $\boldsymbol{0}$ is a suitable null matrix. The matrix $\boldsymbol{B} - \boldsymbol{C}^T(\boldsymbol{A} + \boldsymbol{\sigma}_{\mathrm{M}})^{-1}\boldsymbol{C}$ is the *Schur complement* of the matrix $\boldsymbol{\sigma}$ with respect to $\boldsymbol{A} + \boldsymbol{\sigma}_{\mathrm{M}}$. Now, since

$$\boldsymbol{M}(\boldsymbol{\Lambda}_1, \tilde{\boldsymbol{\Lambda}}) = \left(\boldsymbol{\Lambda}_1 + (\boldsymbol{A} + \boldsymbol{\sigma}_{\mathrm{M}})^{-1}\boldsymbol{C}\tilde{\boldsymbol{\Lambda}}, \tilde{\boldsymbol{\Lambda}}\right), \tag{A.10}$$

Eq. (A.4) becomes

$$\chi'(\tilde{\boldsymbol{\Lambda}}) = \frac{1}{p(\boldsymbol{X})} \exp\left\{-\tfrac{1}{2}\tilde{\boldsymbol{\Lambda}}^T[\boldsymbol{B} - \boldsymbol{C}^T(\boldsymbol{A} + \boldsymbol{\sigma}_{\mathrm{M}})^{-1}\boldsymbol{C}]\, \tilde{\boldsymbol{\Lambda}} - i\tilde{\boldsymbol{\Lambda}}^T \boldsymbol{C}^T(\boldsymbol{A} + \boldsymbol{\sigma}_{\mathrm{M}})^{-1}\boldsymbol{X}\right\}$$

$$\times \int_{\mathbb{R}^2} \frac{d^2\boldsymbol{\Lambda}'}{2\pi^2} \exp\left\{-\tfrac{1}{2}(\boldsymbol{\Lambda}')^T(\boldsymbol{A} + \boldsymbol{\sigma}_{\mathrm{M}})\, (\boldsymbol{\Lambda}') + i(\boldsymbol{\Lambda}')^T \boldsymbol{X}\right\} \tag{A.11}$$

$$= \exp\left\{-\tfrac{1}{2}\tilde{\boldsymbol{\Lambda}}^T[\boldsymbol{B} - \boldsymbol{C}^T(\boldsymbol{A} + \boldsymbol{\sigma}_{\mathrm{M}})^{-1}\boldsymbol{C}]\, \tilde{\boldsymbol{\Lambda}} - i\tilde{\boldsymbol{\Lambda}}^T \boldsymbol{C}^T(\boldsymbol{A} + \boldsymbol{\sigma}_{\mathrm{M}})^{-1}\boldsymbol{X}\right\} \tag{A.12}$$

where we performed the change of variables $\boldsymbol{\Lambda}' = \boldsymbol{\Lambda}_1 + (\boldsymbol{A}+\boldsymbol{\sigma}_{\rm M})^{-1}\boldsymbol{C}\tilde{\boldsymbol{\Lambda}}$. The conditional state $\chi'(\tilde{\boldsymbol{\Lambda}})$ is a $(n-1)$-mode Gaussian state with covariance matrix $\boldsymbol{B}-\boldsymbol{C}^T(\boldsymbol{A}+\boldsymbol{\sigma}_{\rm M})^{-1}\boldsymbol{C}$ and mean value vector $\boldsymbol{C}^T(\boldsymbol{A}+\boldsymbol{\sigma}_{\rm M})^{-1}\boldsymbol{X}$.

Measurement on mode n — Now we focus our attention on mode n and address a measurement described by the characteristic function

$$\chi_{\rm M}(\boldsymbol{\Lambda}_n) = \pi^{-1}\,\exp\left(-\tfrac{1}{2}\boldsymbol{\Lambda}_n^T\boldsymbol{\sigma}_{\rm M}\,\boldsymbol{\Lambda}_n - i\boldsymbol{\Lambda}_n^T\boldsymbol{X}\right), \tag{A.13}$$

where, again, $\boldsymbol{\sigma}_{\rm M}$ is the covariance matrix of the measurement and $\boldsymbol{X}$ the mean values vector. We write the vector $\boldsymbol{\Lambda}$ and the covariance matrix $\boldsymbol{\Sigma}$ of (A.1) as follows:

$$\boldsymbol{\Lambda} = (\boldsymbol{\Lambda}_1,\boldsymbol{\Lambda}_2,\ldots,\boldsymbol{\Lambda}_n) = (\tilde{\boldsymbol{\Lambda}},\boldsymbol{\Lambda}_n), \quad \boldsymbol{\Sigma} = \left(\begin{array}{c|c}\boldsymbol{A} & \boldsymbol{C}\\ \hline \boldsymbol{C}^T & \boldsymbol{B}\end{array}\right), \tag{A.14}$$

where, now, $\boldsymbol{A}\in\mathbb{R}^{\,2(n-1)}\times\mathbb{R}^{\,2(n-1)}$ and $\boldsymbol{B}\in\mathbb{R}^{\,2}\times\mathbb{R}^{\,2}$ are symmetric, and $\boldsymbol{C}\in\mathbb{R}^{\,2(n-1)}\times\mathbb{R}^{\,2}$. The characteristic function of the system after the measurement is given by

$$\chi''(\tilde{\boldsymbol{\Lambda}}) = \frac{1}{p(\boldsymbol{X})}\int_{\mathbb{R}^{\,2}}\frac{d^2\boldsymbol{\Lambda}_n}{2\pi}\chi(\tilde{\boldsymbol{\Lambda}},\boldsymbol{\Lambda}_n)\,\chi_{\rm M}(-\boldsymbol{\Lambda}_n), \tag{A.15}$$

and $p(\boldsymbol{X})$ is

$$p(\boldsymbol{X}) = \frac{1}{(2\pi)^n}\int_{\mathbb{R}^{\,2n}} d^{2(n-1)}\tilde{\boldsymbol{\Lambda}}\,d^2\boldsymbol{\Lambda}_n\,\chi(\tilde{\boldsymbol{\Lambda}},\boldsymbol{\Lambda}_n)\,(2\pi)^{2(n-1)}\delta(-\tilde{\boldsymbol{\Lambda}})\,\times\chi_{\rm M}(-\boldsymbol{\Lambda}_n) \tag{A.16}$$

$$= \int_{\mathbb{R}^{\,2}}\frac{d^2\boldsymbol{\Lambda}_n}{2\pi^2}\,\exp\left[-\tfrac{1}{2}\boldsymbol{\Lambda}_n^T(\boldsymbol{B}+\boldsymbol{\sigma}_{\rm M})\,\boldsymbol{\Lambda}_n + i\boldsymbol{\Lambda}_n^T\boldsymbol{X}\right] = \frac{\exp\left[-\frac{1}{2}\boldsymbol{X}^T(\boldsymbol{B}+\boldsymbol{\sigma}_{\rm M})^{-1}\boldsymbol{X}\right]}{\pi\sqrt{{\rm Det}[\boldsymbol{B}+\boldsymbol{\sigma}_{\rm M}]}}, \tag{A.17}$$

where $\delta(-\tilde{\boldsymbol{\Lambda}}) = \prod_{k=1}^{n-1}\delta^{(2)}(-\boldsymbol{\Lambda}_k)$ is the product of Kronecker deltas in $\mathbb{R}^{\,2}$. We have

$$\chi(\tilde{\boldsymbol{\Lambda}},\boldsymbol{\Lambda}_n)\,\chi_{\rm M}(-\boldsymbol{\Lambda}_n) = \pi^{-1}\,\exp\left[-\tfrac{1}{2}(\tilde{\boldsymbol{\Lambda}},\boldsymbol{\Lambda}_n)^T\boldsymbol{\sigma}\,(\tilde{\boldsymbol{\Lambda}},\boldsymbol{\Lambda}_n) + i\boldsymbol{\Lambda}_n^T\boldsymbol{X}\right], \tag{A.18}$$

where, now,

$$\boldsymbol{\sigma} = \left(\begin{array}{c|c}\boldsymbol{A} & \boldsymbol{C}\\ \hline \boldsymbol{C}^T & \boldsymbol{B}+\boldsymbol{\sigma}_{\rm M}\end{array}\right). \tag{A.19}$$

To perform the integral (A.15) we observe that $\boldsymbol{\sigma}$ can be rewritten as follows:

$$\boldsymbol{\sigma} = \boldsymbol{N}^T\left(\begin{array}{c|c}\boldsymbol{A}-\boldsymbol{C}(\boldsymbol{B}+\boldsymbol{\sigma}_{\rm M})^{-1}\boldsymbol{C}^T & \boldsymbol{0}\\ \hline \boldsymbol{0} & \boldsymbol{B}+\boldsymbol{\sigma}_{\rm M}\end{array}\right)\boldsymbol{N}, \quad \boldsymbol{N} = \left(\begin{array}{c|c}\mathbb{1}_{2(n-1)} & \boldsymbol{0}\\ \hline (\boldsymbol{B}+\boldsymbol{\sigma}_{\rm M})^{-1}\boldsymbol{C}^T & \mathbb{1}_2\end{array}\right). \tag{A.20}$$

The matrix $\boldsymbol{A}-\boldsymbol{C}(\boldsymbol{B}+\boldsymbol{\sigma}_{\rm M})^{-1}\boldsymbol{C}^T$ is the *Schur complement* of the matrix $\boldsymbol{\sigma}$ with respect to $\boldsymbol{B}+\boldsymbol{\sigma}_{\rm M}$. Now, since

$$\boldsymbol{N}(\tilde{\boldsymbol{\Lambda}},\boldsymbol{\Lambda}_n) = \left(\tilde{\boldsymbol{\Lambda}},(\boldsymbol{B}+\boldsymbol{\sigma}_{\rm M})^{-1}\boldsymbol{C}^T\tilde{\boldsymbol{\Lambda}}+\boldsymbol{\Lambda}_n\right), \tag{A.21}$$

Eq. (A.15) becomes

$$\chi''(\tilde{\boldsymbol{\Lambda}}) = \frac{1}{p(\boldsymbol{X})}\,\exp\left\{-\tfrac{1}{2}\tilde{\boldsymbol{\Lambda}}^T[\boldsymbol{A}-\boldsymbol{C}(\boldsymbol{B}+\boldsymbol{\sigma}_{\rm M})^{-1}\boldsymbol{C}^T]\,\tilde{\boldsymbol{\Lambda}} - i\tilde{\boldsymbol{\Lambda}}^T\boldsymbol{C}(\boldsymbol{B}+\boldsymbol{\sigma}_{\rm M})^{-1}\boldsymbol{X}\right\}$$
$$\times\int_{\mathbb{R}^{\,2}}\frac{d^2\boldsymbol{\Lambda}'}{2\pi^2}\exp\left\{-\tfrac{1}{2}(\boldsymbol{\Lambda}')^T(\boldsymbol{B}+\boldsymbol{\sigma}_{\rm M})\,(\boldsymbol{\Lambda}')+i(\boldsymbol{\Lambda}')^T\boldsymbol{X}\right\} \tag{A.22}$$

$$= \exp\left\{-\tfrac{1}{2}\tilde{\boldsymbol{\Lambda}}^T[\boldsymbol{A}-\boldsymbol{C}(\boldsymbol{B}+\boldsymbol{\sigma}_{\rm M})^{-1}\boldsymbol{C}^T]\,\tilde{\boldsymbol{\Lambda}} - i\tilde{\boldsymbol{\Lambda}}^T\boldsymbol{C}(\boldsymbol{B}+\boldsymbol{\sigma}_{\rm M})^{-1}\boldsymbol{X}\right\} \tag{A.23}$$

where we performed the change of variables $\boldsymbol{\Lambda}' = \boldsymbol{\Lambda}_1 + (\boldsymbol{B}+\boldsymbol{\sigma}_{\rm M})^{-1}\boldsymbol{C}^T\tilde{\boldsymbol{\Lambda}}$. The conditional state $\chi''(\tilde{\boldsymbol{\Lambda}})$ is a $(n-1)$-mode Gaussian state with covariance matrix $\boldsymbol{A}-\boldsymbol{C}(\boldsymbol{B}+\boldsymbol{\sigma}_{\rm M})^{-1}\boldsymbol{C}^T$ and mean value vector $\boldsymbol{C}(\boldsymbol{B}+\boldsymbol{\sigma}_{\rm M})^{-1}\boldsymbol{X}$.

References

1. A. Ferraro, M.G.A. Paris, Phys. Rev. A **72**, 032312 (2005)
2. A. Ferraro, M.G.A. Paris, J. Opt. B: Quantum Semiclass. Opt. **7**, 174 (2005)
3. M. Murao et al., Phys. Rev. A **59**, 156 (1999)
4. N. Cerf, A. Ipe, X. Rottenberg, Phys. Rev. Lett. **85**, 1754 (2000)
5. V. Scarani et al., Rev. Mod. Phys. **77**, 1225 (2005)
6. F. Dell'Anno, S. De Siena, F. Illuminati, Phys. Rep. **428**, 53 (2006)
7. F. Grosshans, P. Grangier, Phys. Rev. A **6401**, 010301 (2001)
8. J. Fiuràšek, Phys. Rev. A **66**, 012304 (2002)
9. S. Olivares, M.G.A. Paris, R. Bonifacio, Phys. Rev. A **67**, 032314 (2003)
10. S. Olivares, M.G.A. Paris, Phys. Rev. A **70**, 032112 (2004)
11. S. Pirandola, S. Mancini, D. Vitali, Phys. Rev. A **71**, 042326 (2005)
12. A. Ferraro, et al., J. Opt. Soc. Am. B **21**, 1241 (2004)
13. M. Bondani et al., Opt. Lett. **29**, 180 (2004)
14. A.S. Bradley, M.K. Olsen, O. Pfister et al., Phys. Rev. A **72**, 053805 (2005); R.C. Pooser, O. Pfister, Opt. Lett. **30**, 2635 (2005)
15. A.V. Rodionov, A.S. Chirkin, JETP Lett. **79**, 582 (2004); M.K. Olsen, A.S. Bradley, J. Phys. B: At. Mol. Opt. Phys. **39**, 127 (2006)
16. S. Olivares, Phys. Rev. A **76**, 022305 (2007)
17. A. Ferraro, S. Olivares, M.G.A. Paris, *Gaussian States in Quantum Information*, Napoli Series on Physics and Astrophysics (Bibliopolis, Napoli, 2005) [`e-print quant-ph/0503237`]
18. M.E. Smithers, E.Y.C. Lu, Phys. Rev. A **10**, 1874 (1974)
19. M.M. Cola, M.G.A. Paris, N. Piovella, Phys. Rev. A **70**, 043809 (2004)
20. G. Giedke et al., Phys. Rev. A **64**, 052303 (2001)